Luminescence Studies with *trp* Repressor and Its Single-Tryptophan Mutants†

Maurice R. Eftink* and Glen D. Ramsay

Department of Chemistry, University of Mississippi, University, Mississippi 38677

Laura Burns and August H. Maki

Department of Chemistry, University of California, Davis, California 95616

Craig J. Mann and C. R. Matthews

Department of Chemistry, Pennsylvania State University, University Park, Pennsylvania 16802

Camillo A. Ghiron

Department of Biochemistry, University of Missouri, Columbia, Missouri 65201

Received March 4, 1993; Revised Manuscript Received June 8, 1993®

ABSTRACT: Time-resolved and steady-state fluorescence, low-temperature phosphorescence, and optically detected magnetic resonance (ODMR) measurements have been made to resolve the luminescence contributions of the two intrinsic tryptophan residues in the subunits of *trp* aporepressor from *Escherichia coli*. Assignments of spectral information have been confirmed by use of the single-tryptophan mutants W19F and W99F. Solute fluorescence quenching studies show that both Trp19 and Trp99 are exposed to acrylamide and iodide, with Trp99 being the more exposed. Time-resolved and steady-state fluorescence measurements show Trp19 to have a bluer emission, a longer mean fluorescence decay time, a higher quantum yield, and essentially no independent rotational motion with respect to the protein. Trp99 is found to have a redder emission, a shorter mean fluorescence decay time, a lower quantum yield, and a significant degree of rotational freedom. Phosphorescence studies show a clear resolution of 0–0 vibronic transitions for each type of residue, with maxima at 407 and 415 nm that are assigned to Trp19 and Trp99, respectively. ODMR measurements show the zero-field splitting parameters to be quite characteristically different for each tryptophan residue. The existence of resonance energy transfer from Trp19 to Trp99, in the wild-type protein, is indicated by three types of data: comparison of the long-lived decay time (attributed to Trp19) in the absence (W99F) and presence (wild type) of the acceptor Trp99, comparison of the fluorescence quantum yield of the wild-type and mutant proteins, and deviations from the expected phosphorescence intensities for Trp19 and Trp99 in the absence of energy transfer.

Tryptophan aporepressor (apo-trpR)[1] from *Escherichia coli* is a symmetrical dimeric protein. Upon binding the corepressor, tryptophan, it interacts with at least three operator DNA segments to block the transcription of operons involved in the biosynthesis of tryptophan, other aromatic amino acids, and apo-trpR itself (Zurawski *et al.*, 1981). TrpR has been extensively studied in recent years as an example of a nucleic acid binding protein. The crystal structure has been reported for trpR, its binary complex with tryptophan and indolepropionic acid, and its ternary complex with operator (Zhang *et al.*, 1987; Otwinowski *et al.*, 1988; Lawson & Sigler, 1988). Thermodynamic studies have been reported for the interaction between trpR, various tryptophan analogs, and operator DNA (Marmorstein *et al.*, 1987; Marmorstein & Sigler, 1989; Carey, 1988; Chou *et al.*, 1989).

There are two intrinsic tryptophan residues, Trp19 and Trp99, in each subunit. In this paper we explore the use of the fluorescence of these tryptophan residues to probe the structure and dynamics of trpR. To do so, we must resolve and assign the fluorescence properties of these proteins. Time-resolved and steady-state fluorescence, low-temperature phosphorescence, and optically detected magnetic resonance (ODMR) studies are presented. We show here that such an assignment can be facilitated by measurements of low-temperature phosphorescence and/or ODMR, for which the 0–0 triplet → singlet transition of tryptophans in different environments can often be resolved. Single tryptophan mutant

† This research was supported by NSF Grant DMB 91-06377 to M.R.E., NIH Grant ES-02662 to A.H.M., NIH Grant GM-23303 to C.R.M., and NIH Postdoctoral Fellowship Award GM13571 to C.J.M.

® Abstract published in *Advance ACS Abstracts,* August 15, 1993.

[1] Abbreviations: α_i, preexponential factor associated with fluorescence decay time τ_i; D and E, zero-field splitting parameters of the triplet state; E_T, degree of energy transfer; F and F_o, steady-state fluorescence intensity in the presence and absence of quencher; f_i, fractional steady-state fluorescence intensity, equal to $\alpha_i\tau_i/\sum\alpha_i\tau_i$; Φ, quantum yield (i.e., for fluorescence); K_Q, K_A, K_I, Stern–Volmer quenching constants for general quencher (Q), acrylamide (A), or iodide (I); k_f, rate constant for fluorescence decay of an excited singlet state; k_{nf}, rate constant for nonradiative deactivation of an excited singlet state; k_{ic}, rate constant for intersystem crossing from an excited singlet state to a triplet state; k_{DA}, rate constant for resonance energy transfer between the excited singlet state of a donor and an excited singlet state of an acceptor; k_p, rate constant for phosphorescence decay from a triplet state; k_{np}, rate constant for nonradiative deactivation of a triplet state; ODMR, optically detected magnetic resonance; ϕ_i, rotational correlation time for species i; g_ir_o, amplitude of anisotropy decay associated with species i; [Q], concentration of quencher; τ_i, fluorescence decay time for component i; $\langle\tau\rangle$, mean fluorescence decay time, equal to $\sum\alpha_i\tau_i$; trpR, *trp* aporepressor from *E. coli*; WT, wild-type trpR; W19F, single-point mutant with phenylalanine substituted for tryptophan at position 19 in both subunits; W99F, single-point mutant with phenylalanine substituted for tryptophan at position 99 in both subunits.

0006-2960/93/0432-9189$04.00/0

proteins are also studied; these enable the confirmation of the assignments of fluorescence and phosphorescence contributions from Trp19 and Trp99.

EXPERIMENTAL PROCEDURES

Materials. The procedures used to perform site-directed mutagenesis are described elsewhere (Mann *et al.*, 1993). The wild-type and mutant proteins were purified from an overproducing *E. coli* strain (Joachimiak *et al.*, 1983; Paluh & Yanofsky, 1986; Chou *et al.*, 1989). Single bands were found on sodium dodecyl sulfate–polyacrylamide gels. Frozen protein samples were dialyzed or diluted into the appropriate buffer before use. Unless specified, the buffer was 0.1 M KCl, 0.02 M potassium phosphate, and 0.001 M EDTA, pH 7.5. Protein concentration was determined using a molar extinction coefficient of $\epsilon_{280} = 1.5 \times 10^4$ M^{-1} cm^{-1} per subunit of the wild-type apo-trpR, 8.2×10^3 M^{-1} cm^{-1} for W19F, and 8.2×10^3 M^{-1} cm^{-1} for W99F (Mann *et al.*, 1993).

Glycerol (Sigma Chemical Co.) and ethylene glycol (Fluka Chemical Co.) were used without further purification.

Methods. Steady-state fluorescence measurements are uncorrected and were made on a Perkin-Elmer (Norwalk, CT) MPF44A spectrophotofluorometer, with the sample in a thermojacketed cell holder maintained at 20 °C. Excitation was at 295 nm, unless specified otherwise. Acrylamide and iodide solute quenching studies were performed by adding aliquots from a concentrated (8 and 5 M, respectively) solution of quencher into a cuvette containing the protein. Corrections for dilution of the protein and absorptive screening (by acrylamide) were made as described previously (Eftink & Ghiron, 1976). Fluorescence quenching data were analyzed according to the following general form of the Stern–Volmer equation:

$$F/F_o = \sum f_i/((1 + K_{SV,i}[Q]) \exp(V_i[Q])) \qquad (1)$$

where F and F_o are the fluorescence intensities in the presence and absence of quencher, f_i is the fractional intensity corresponding to component i, $K_{SV,i}$ is the dynamic quenching constant (equal to $k_q\langle\tau\rangle_o$, where k_q is the quenching rate constant and $\langle\tau\rangle_o$ is the mean fluorescence lifetime in the absence of quencher) for component i, V_i is the static quenching constant for component i, and [Q] is the total quencher concentration (Eftink & Ghiron, 1976; Eftink, 1991b). Inclusion of the $\exp(V_i[Q])$ term in the above equation applies in cases where there is upward curvature in a Stern–Volmer (F_o/F vs [Q]) plot, due to static quenching, as is often found with acrylamide as quencher (see Figure 2A). For iodide as quencher, the Stern–Volmer plots that we obtain (see Figure 2B) are downward curving, and the data were analyzed in terms of a two-component Stern–Volmer equation without inclusion of the static term. Quenching data were fitted to various versions of the above general Stern–Volmer equation by a nonlinear least squares program.

Low-temperature phosphorescence spectra were obtained on a Farrand (New York) Mark V fluorometer with a phosphorescence attachment and a liquid nitrogen quartz finger dewar. The protein samples were made to be ≈50% glycerol (by weight), and were placed in a 3-mm-diameter spin tube, degassed by batch sonication, and frozen to a glass at 77 K for spectral measurements. On some occasions, an amount of KI was added to perturb the signal. Either phosphorescence or total luminescence spectra were recorded.

Time-resolved intensity decay and anisotropy decay data were obtained using an ISS (Champaign, IL) phase/modulation frequency domain fluorometer. This instrument is equipped with a 20-W argon ion laser (Coherent Inc., Palo Alto, CA) having a deep UV output at 300 nm. The laser beam is modulated over the frequency range 5–200 MHz by a Pockels cell modulator. The acquisition of phase and modulation data is under computer control. As a reference standard, *p*-terphenyl (τ = 1.0 ns) was used. The emission was collected through WG 335 and Corning 7–60 filters, and the sample temperature was controlled at 20 °C. "Magic angle" detection was not used for most intensity decay measurements; a couple of measurements were made with an emission polarizer set at 55°, and no significant difference in the fitted τ_i values was detected. For differential polarized phase/modulation (anisotropy decay) measurements, Glan–Thomson polarizers were inserted.

The intensity decay data were analyzed in terms of the following multiexponential decay law:

$$I(t) = I_o \sum \alpha_i \exp(-t/\tau_i) \qquad (2)$$

where α_i and τ_i are the normalized preexponential factor and decay time associated with fluorescence component i. The mean lifetime, $\langle\tau\rangle$, is defined as $\langle\tau\rangle = \sum\alpha_i\tau_i$, and the fractional fluorescence intensity of each component is defined as $f_i = \alpha_i\tau_i/\sum\alpha_i\tau_i$. Data analyses were performed with a nonlinear least squares program from ISS or with GLOBALS Unlimited (Beechem *et al.*, 1991). The latter program was used to perform a simultaneous, linked analysis of iodide quenching data. That is, the τ_i for multiple data sets were given by $1/\tau_i = 1/\tau_{oi} + k_{qi}[Q]$, where τ_{oi} is the component lifetime in the absence of quencher. Anisotropy decay data were analyzed using the following equation:

$$r(t) = r_o \sum g_i \exp(-t/\phi_i) \qquad (3)$$

where r_o is the anisotropy in the absence of depolarizing processes, and g_i and ϕ_i are the preexponential factor and rotational correlation time for component i. Again, the software for data analysis was either ISS or GLOBALS. A nonassociated analysis was performed.

Slow-passage ODMR measurements were performed with an instrument described elsewhere (Maki, 1984). Briefly, these measurements were made at pumped liquid helium temperature (1.2 K) on protein samples ($\sim 5–10 \times 10^{-5}$ M) in 20% (by volume) ethylene glycol in a quartz sample tube (1-mm i.d.), which was placed in a dewar equipped with optical ports. The sample was suspended in a microwave slow wave copper helix terminating a coaxial transmission line. Microwaves were generated using a Hewlett-Packard 8350B microwave sweep oscillator with a Model 8359A plug-in, capable of generating microwaves in the 0.1–20-GHz region. Exciting light (295 nm), provided by a 100-W mercury arc lamp, was selected by an Instruments SA monochromater (16-nm band-pass) and was passed through a 12-cm $NiSO_4$ solution (500 mg/L) to filter the IR. Slow-passage ODMR signals in zero applied magnetic field were obtained by monitoring the change in steady-state phosphorescence (detected at right angles via a 1-m monochromater (McPherson Model 2051) and a cooled photomultiplier tube) as microwave frequencies were swept through the triplet-state zf transitions. The condition for slow passage generally requires the sweep duration to be $\geq 5\tau$, where τ is the lifetime of the longest lived sublevel. The wavelength dependence of the slow-passage triplet-state transitions was determined by collecting signals at 1.5-nm intervals across the 0–0 band with an emission resolution of 1.5 nm. The position of slow-passage resonances depends on the sweep rate; this effect was compensated by extrapolation of peak frequencies to zero sweep rate.

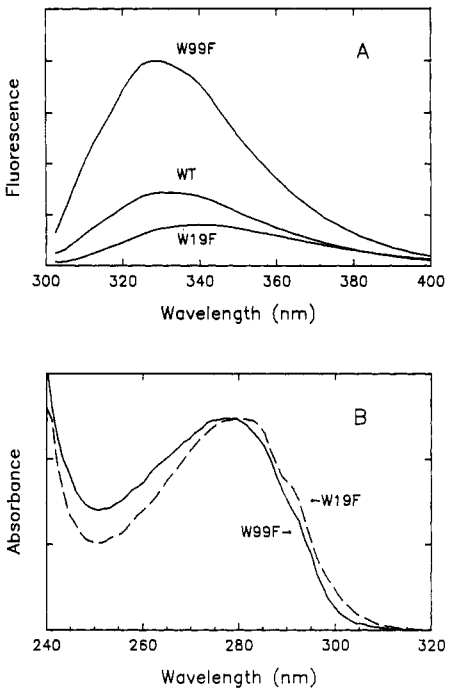

FIGURE 1: (A) Fluorescence spectra (uncorrected) of WT, W19F, and W99F trpR at 20 °C, pH 7.5, with excitation at 295 nm. The three spectra have approximately the same absorbance at 295 nm. (B) Absorbance spectra for W19F (– –) and W99F (—).

RESULTS

Steady-State Fluorescence Data. The fluorescence spectra of wild-type apo-trpR (WT) and the W19F and W99F mutants are shown in Figure 1A. WT has a maximum at about 332 nm. The W19F and W99F mutants are slightly red and blue shifted, respectively, in their emission maxima, and the fluorescence quantum yields of W19F and W99F are smaller and larger, respectively, than that of WT. Various fluorescence parameters for the three proteins are listed in Table I. The absorbance spectra of the two mutants (Figure 1B) show that the absorbance of Trp99 in W19F is redder than that of Trp19 of W99F.

Fluorescence quenching studies with acrylamide and KI are shown as the Stern–Volmer plots in Figure 2. The acrylamide Stern–Volmer plots for the three proteins have a slight upward curvature and were fitted to eq 1 (single component) with inclusion of the static quenching term. The fitting parameters are given in Table II. The greatest degree of quenching is seen for W19F, with WT and W99F showing a similar degree of quenching by acrylamide. Dividing the apparent K_{SV} by the mean fluorescence lifetime, $\langle\tau\rangle$ (see below), we obtain quenching rate constants, k_q, of 1.95, 4.5, and 0.97×10^9 M^{-1} s^{-1} for WT, W19F, and W99F, respectively. The iodide Stern–Volmer plots (Figure 2B) show a downward curvature for each protein, with the degree of quenching decreasing in the order W19F, WT, and W99F. The downward curvature is easily interpreted in terms of heterogeneous emission from the two types of tryptophan residues in WT. For the two mutants, the downward curvature may be attributed to an electrostatic interaction with the protein surface (which is not shielded by the initial ionic strength of 0.1 M) or to the heterogeneity in the fluorescence decay time (see below) for these single (class) tryptophan containing mutants. Taking the initial slopes of the iodide Stern–Volmer plots as $K_{SV}(\text{effective}) = \sum f_i K_{SV,i}$ and the mean fluorescence lifetime, $\langle\tau\rangle$, effective quenching rate constants of 2.45, 3.4, and 1.6×10^9 M^{-1} s^{-1} are found for WT, W19F, and W99F, respectively. Thus, both the neutral quencher, acrylamide, and the anionic quencher, iodide, reveal Trp99, which remains

Table I: Luminescence Properties of Wild-Type apo-trpR, W19F, and W99F

	WT	W19F	W99F
	Fluorescence		
λ_{max} (nm)	332	339	328
quantum yield	0.063	0.039	0.164
lifetime			
τ_1 (ns)	3.36	3.14	3.94
α_1	0.30	0.17	0.72
f_1	0.716	0.526	0.962
τ_2 (ns)	0.57	0.58	0.40
α_2	0.70	0.83	0.28
f_2	0.284	0.474	0.038
mean $\langle\tau\rangle$	1.41	1.01	2.95
mean k_f ($\times 10^{-9}$ s^{-1})		0.068	0.215
mean k_{nf} ($\times 10^{-9}$ s^{-1})		0.922	0.038
iodide k_q ($\times 10^{-9}$ M^{-1} s^{-1})	2.45	3.4	1.6
acrylamide k_q ($\times 10^{-9}$ M^{-1} s^{-1})	1.95	4.5	0.97
rotational correlation time, ϕ_1 (ns)	14.3	15 ± 5	13.0
$g_1 r_o$	0.257	0.19	0.253
ϕ_2 (ns)	0.25	0.8 ± 0.3	
$g_2 r_o$	0.06	0.10	
	Phosphorescence and ODMR		
0–0 transition (nm)	407 415	415	407
lifetime (s)	5.9 (407 nm) 5.6 (415 nm)	6.0	6.1
$D - E$ (GHz)	1.79 (407 nm) 1.61 (415 nm)	1.60	1.79
(bandwidth (MHz))		(35)	(100)
$2E$ (GHz)	2.47 (407 nm) 2.71 (415 nm)	2.72	2.49
(bandwidth (MHz))		(140)	(180)

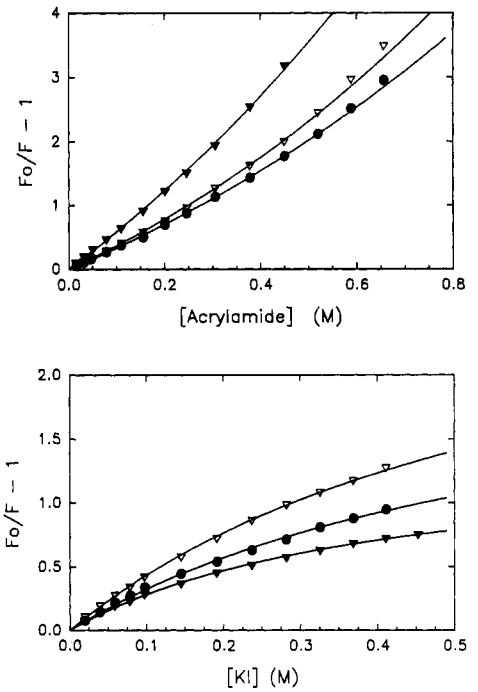

FIGURE 2: (A, top) Stern–Volmer plots for the acrylamide quenching of the steady-state fluorescence of WT (●), W19F (▲), and W99F trpR (△) at 20 °C, pH 7.5 (0.02 M sodium phosphate, 0.1 M KCl), with excitation at 295 nm and emission at the maximum. The solid lines are fits of eq 1 with parameters given in Table II. (B, bottom) Stern–Volmer plots for the KI quenching of the fluorescence of WT (●), W19F (▲), and W99F (△), with conditions as above. The solid lines are fits to eq 1 (without the inclusion of static quenching; a two-component model with one component assumed to be unquenchable) with the parameters given in Table II.

Table II: Solute Fluorescence Quenching Parameters for Wild-Type trpR, W19F, and W99F

	Iodide Quencher			
	$K_{I,1}$ (M^{-1})	$K_{I,2}$ (M^{-1})	f_1	SSR
WT	5.34	⟨0⟩	0.705	2.35×10^{-4}
	2.70		⟨1.0⟩	9.7×10^{-4}
W19F	5.99	⟨0⟩	0.588	7.9×10^{-5}
	2.08		⟨1.0⟩	1.6×10^{-3}
W99F	6.64	⟨0⟩	0.761	9.1×10^{-5}
	3.7		⟨1.0⟩	9.3×10^{-4}

	Acrylamide Quencher		
	K_A (M^{-1})	V_A (M^{-1})	SSR
WT	2.74	0.48	3.6×10^{-5}
W19F	5.14	0.48	1.7×10^{-4}
W99F	2.87	0.62	3.6×10^{-5}

[a] Quenching studies performed at pH 7.5, 0.1 M KCl, 0.02M K phosphate, 20 °C. Iodide quenching data were fitted to either a two-component model (eq 1 with no static quenching) with K_2 fixed at 0 (i.e., quenching of only one component) or a single-component model. The $K_{I,eff}$ used to calculate $k_{q,I}$ in Table I is $K_{I,eff} = \sum f_i K_{I,i}$. Acrylamide quenching data were fitted to a single-component model including static quenching (eq 1 with $i = 1$). Subscripts I and A refer to iodide and acrylamide as quenchers. SSR is the sum of the squares of the residuals for the fit. Angle brackets, ⟨ ⟩, indicate a parameter that was fixed.

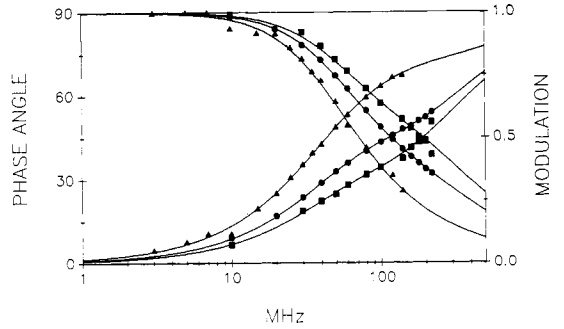

FIGURE 3: Phase/modulation fluorescence lifetime data for WT (●), W19F (■), and W99F trpR (▲) at 20 °C, pH 7.5, in 0.15 M KCl and 0.02 M potassium phosphate. The solid lines are fits to a biexponential decay (eq 2) with the parameters given in Table I.

in W19F, to be the most exposed. Trp19, which remains in W99F, is still partially exposed to the quenchers, having a k_q that is lower only by a factor of 2–5 compared to Trp99 for both quenchers. The quenching patterns for WT are intermediate or more like that of Trp19 (in W99F), suggesting the dominance of this tryptophan residue in the fluorescence of WT.

Time-Resolved Fluorescence Data. Phase/modulation fluorescence lifetime data for WT and the two mutants are shown in Figure 3. In each case the decay is a nonexponential. The fitting parameters for a biexponential are given in Table I. The wild type has contributions from both a 3.3-ns component and a 0.7-ns component. The decay of W19F is dominated by a 0.5-ns component, and the decay of W99F is dominated by a 3.9-ns component, although in both cases there is a contribution from other components. The mean lifetime, $\langle\tau\rangle = \sum\alpha_i\tau_i$, for each protein is also listed in Table I. To a first approximation, the fluorescence decay of WT is a combination of the decays of the two mutants (see Discussion for the possibility of energy transfer).

Phase/modulation data were also collected for WT as a function of the quencher, KI, concentration from 0 to 1.0 M (with the ionic strength maintained at 1.0 M). These data (not shown) were analyzed by linking the τ_i values to follow a dynamic Stern–Volmer equation and by linking α_i to be

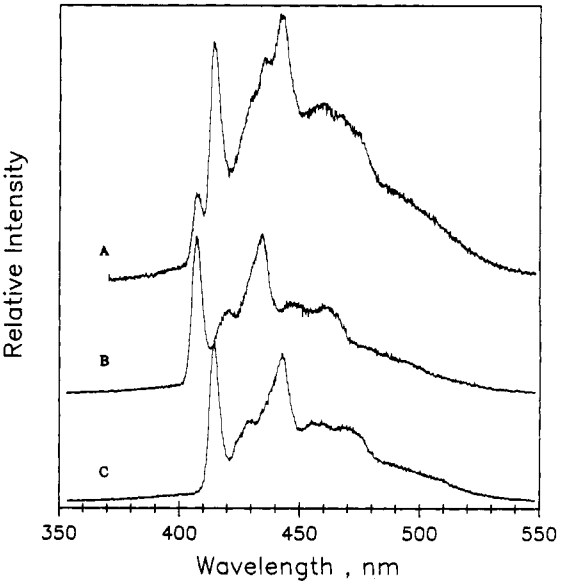

FIGURE 4: Low-temperature phosphorescence spectra of WT (A), W99F (B), and W19F trpR (C) at liquid nitrogen temperature. The spectra are offset for visualization.

constant at all [Q]. The analysis showed both putative lifetime components to be dynamically quenched with similar k_q values (in the range $0.2–0.5 \times 10^9$ M^{-1} s^{-1}). The apparent similarity of the k_q values makes their analysis uncertain by time-resolved methods.

Differential polarized phase/modulation anisotropy decay data were obtained for the three proteins (data not shown). Using the fluorescence lifetime parameters given above, these data were analyzed to obtain the rotational correlation times, ϕ_i, and amplitudes, $g_i r_o$, listed in Table I. Trp19 in W99F appears to decay with a single rotational correlation time of ~13 ns. For a spherical protein of molecular mass, M, equal to 25 kDa and having an amount of hydration, h, of 0.3 mL/g and a specific volume, v, of 0.73 mL/g, a rotational correlation time is calculated to be 11 ns (calculated as $\phi_{calc} = M(v + h)\eta/kT$, where η is the bulk viscosity of water). Thus the experimental ϕ for W99F is only slightly larger than the expected value for global rotation of the dimeric protein. The anisotropy decay of Trp99 in W19F is more complicated and is faster. For a forced monoexponential fit, the value of ϕ is 4.9 ns for W19F. A biexponential decay analysis produces $\phi_1 = 15 \pm 5$ ns ($g_1 r_o = 0.19$) and $\phi_2 = 0.8 \pm 0.3$ ns ($g_2 r_o = 0.10$). Thus the motion of Trp99 is chararcterized by more rapid and extensive side-chain motion. For WT, the anisotropy decay is dominated by a $\phi_1 = 14$ ns component, but also has a small contribution from a shorter, $\phi_2 = 0.25$ ns, component.

Low-Temperature Phosphorescence Data. Shown in Figure 4 is the low-temperature (77 K) phosphorescence spectrum of WT. This spectrum was taken with excitation at 295 nm and thus displays only contributions from the tryptophan residues. Two 0–0 transition bands, a smaller one at 407 nm and a larger one at 415 nm, are clearly evident for WT. The ratio of the height of the 407-nm peak to that of the 415-nm peak was reproducibly found to be 0.30–0.35 (using <2-nm emission slits and an excitation wavelength of 295 nm). At a higher temperature of 193 K (dry ice in methanol), there is a decreased resolution of the 407- and 415-nm peaks and a general decrease in the phosphorescence signal. There does not appear, however, to be a selective thermally activated quenching of either the 407- or the 415-nm peak.

Also shown in Figure 4 are low-temperature phosphorescence spectra for the two mutants, W19F and W99F. The

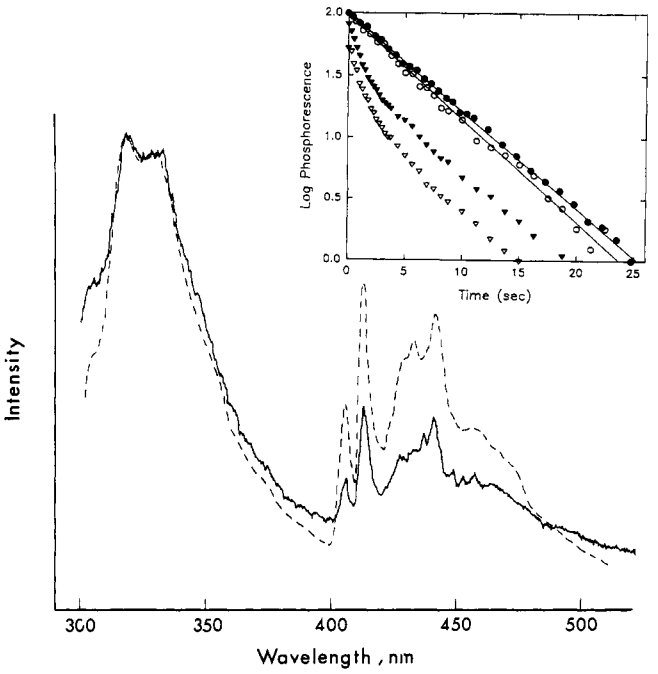

FIGURE 5: Iodide perturbation of the low-temperature total luminescence spectrum of WT trpR. Spectra are shown in the absence (—) and presence (– –) of 0.048 M KI. Inset: Low-temperature phosphorescence decay of WT trpR monitored at 407 (○) and 415 nm (●). Also shown are decays of the 407- (▽) and the 415-nm peak (▼) in the presence of 0.048 M KI. Note that the decays are nonexponential in the presence of KI and have final slopes equal to those in the absence of KI, as expected for Dexter-type quenching kinetics in a frozen solution.

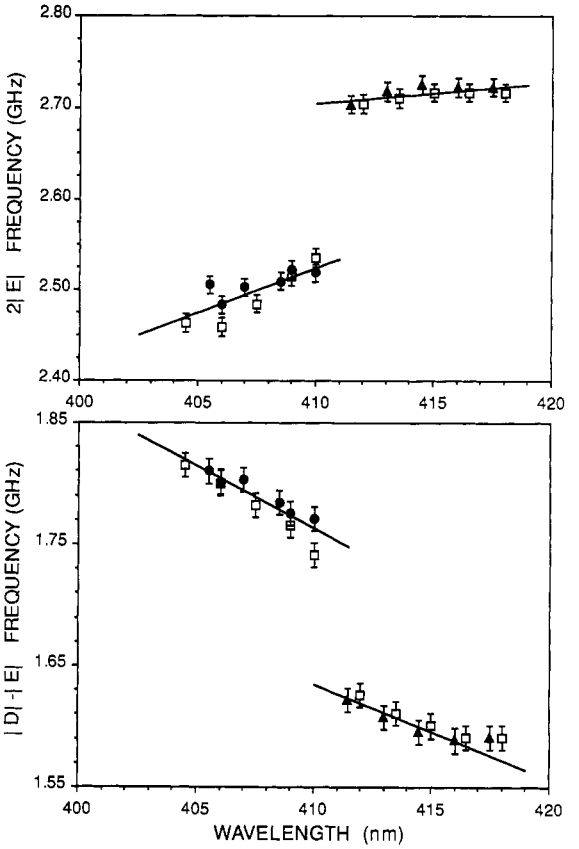

FIGURE 6: Wavelength dependence of the $|D| - |E|$ and $2|E|$ zfs for triplet-state ODMR frequencies within the 0–0 band for WT (□), W19F (▲), and W99F trpR (●) at 1.2 K. The sample contained 20% (by volume) ethylene glycol. Excitation was at 295 nm, and emission resolution was 1.5 nm. All zfs parameters have been corrected for rapid-passage effects.

mutants each show only a single 0–0 transition. These transitions are at 407 nm for Trp19 in W99F and at 415 nm for Trp99 in W19F. Thus the phosphorescence spectrum of WT is a sum of the contributions from the two types of tryptophan residues. (This is further illustrated by Figure 7, which expands the spectra in the 400–420-nm range, and Figure 8, in which the WT spectrum is simulated by a linear superposition of the spectra of the two mutants. See Discussion.)

As the excitation wavelength for WT is increased from 280 to 305 nm, the ratio of the 407/415-nm peaks decreases from 0.35 to 0.25. This indicates that the absorption spectrum of the 415-nm component (Trp99) is the more red shifted.

The phosphorescence decay time of both mutants is 5–6 s at 77 K, a value that is typical of tryptophan at this temperature. For WT, measurement of the phosphorescence decays at 407 and 415 nm gave indistinguishable decay times, as shown in Figure 5 (inset). Also we studied the effect on the phosphorescence spectra and decays of the addition of the heavy atom quencher KI. This agent quenches the fluorescence (singlet state) by promoting intersystem crossing to the triplet state (also it promotes the radiative transition from the triplet to the ground singlet state). Consequently, the addition of KI should actually enhance the phosphorescence of an accessible tryptophan residue (and reduce its phosphorescence decay time) (Li *et al.*, 1992). Shown in Figure 5 is the total luminescence spectrum of WT in the absence (solid line) and presence (dashed line) of 50 mM KI. An enhancement in the phosphorescence/fluorescence ratio is seen. In addition, there is a greater enhancement in the 407-nm peak, compared to the enhancement of the 415-nm peak. One explanation of this observation is that the 407-nm peak is more exposed to iodide, which is randomly distributed in the frozen solution. Another explanation, elaborated upon in the Addendum section, is that the relative enhancement of the 407-nm peak is due to a competition between the intersystem crossing rate (enhanced by the heavy iodide ion) and a resonance energy transfer (singlet level) from Trp19 to Trp99.

Optically Detected Magnetic Resonance. Slow-passage zero-field splitting (zfs) parameters have been determined for the 0–0 band region for the WT and mutant proteins at 1.2 K. The zfs parameters, $|D| - |E|$ and $2|E|$, were found to be different for Trp19 of W99F and Trp 99 of W19F (see Table I), whereas WT has contributions from both types of residues, as shown in Figure 6. For Trp19 of W99F the $|D| - |E|$ and $2|E|$ values are 1.79 and 2.50 GHz, respectively. For Trp99 of W19F, the $|D| - |E|$ and $2|E|$ values are 1.60 and 2.71 GHz, respectively. Figure 6 shows that the zfs data for WT (open symbols) are in excellent agreement with the data for the mutants. Within experimental error, the zfs parameters for WT are identical to those for Trp19 in the wavelength range 404–410 nm and are identical to those for Trp99 in the wavelength range 412–418 nm. For both types of tryptophan residues, there is a small wavelength dependence of the $|D| - |E|$ and $2|E|$ values.

DISCUSSION

Strategy. One of the challenges in the use of intrinsic tryptophan fluorescence as a probe for protein structure, dynamics, and function is to assign spectral contributions to individual tryptophan residues when there are more than one type of residue in a protein (Royer *et al.*, 1990). The present study involves a two-tryptophan protein, apo-trpR (a homodimer). The assignment of contributions of the individual

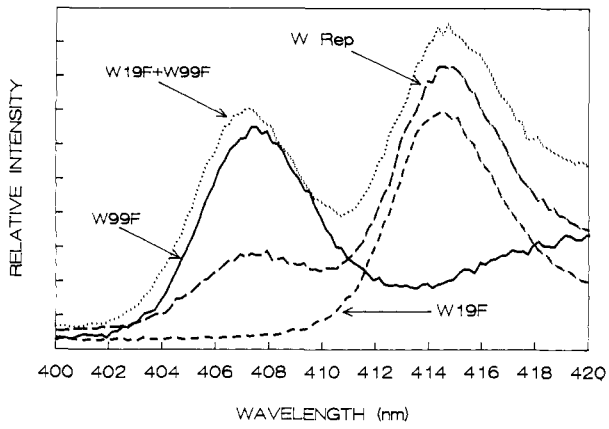

FIGURE 7: Phosphorescence spectra in the 400–420-nm region for W19F (- - -), W99F (—), an equimolar solution of the two mutants (···), and WT trpR (– –). Sample concentration was 6.8×10^{-5} M in each case, and the temperature was 77 K. Excitation for all samples was 295 nm with a 16-nm band-pass. Emission band-pass was 1.5 nm.

tryptophan residues (Trp19 and Trp99) is validated by the availability of two single-tryptophan mutants, W19F and W99F, and involves the use of triplet-state information from low-temperature phosphorescence and ODMR studies. Whereas the fluorescence of individual tryptophan residues in a protein is overlapping and difficult to resolve (i.e., by time-resolved studies and selective solute quenching), the phosphorescence of individual tryptophan residues can sometimes be clearly resolved due to the sharpness of the 0–0 triplet → singlet transition (Purkey & Galley, 1970).

A second challenge in the use of intrinsic fluorescence is to determine the extent to which there is a coupling between the emission of the individual tryptophan residues due to resonance energy transfer. In the absence of such homotransfer, the fluorescence of a protein should be the sum (or average) of the contributions from the various emitting centers. If energy transfer occurs, the fluorescence contributions from individual centers become difficult to dissect.

In the following we will discuss the assignment of contributions to the individual tryptophan residues in trpR, on the basis of time-resolved and steady-state fluorescence studies and low-temperature phosphorescence and ODMR studies. We will discuss the characteristics of each luminescing center, and then we will discuss the evidence for the existence of resonance energy transfer between Trp19 and Trp99 in WT. We note that Royer has recently performed related fluorescence studies with trpR and the same two mutants (Royer, 1992). We present data that are supplementary to her work and generally are consistent with her interpretations of the assignments of contributions.

Assignments. The crystal structure of apo-trpR (Zhang *et al.*, 1987; Otwinowski *et al.*, 1988; Lawson & Sigler, 1988) and NMR studies (Arrowsmith *et al.*, 1989) show that Trp19 is located as part of the A α-helix that forms an apolar core at the subunit interface of this protein and that Trp99 is part of the *F* α-helix and has more surface exposure.

The observation of two 0–0 phosphorescence peaks in WT is consistent with such a difference in microenvironment for the two types of tryptophan residues. For example, another protein having clearly resolved 0–0 phosphorescence transitions for two tryptophan residues with distinctly different microenvironments is horse liver alcohol dehydrogenase (Purkey & Galley, 1970; Eftink, 1992). Studies of the low-temperature phosphorescence of tryptophan residues in proteins have revealed a reverse Stokes shift pattern for the triplet state (Purkey & Galley, 1970; Hershberger *et al.*, 1980; von Schutz *et al.*, 1974; Kwiram & Ross, 1982; Lam *et al.*, 1992). That is, buried tryptophan residues usually tend to have a red-shifted phosphorescence, due to the polarizable nature of the protein interior (which stabilizes the triplet state); solvent-exposed tryptophan residues usually have a bluer phosphorescence, due to the low polarizability and destabilizing effect of the rigid polar solvent on the excited-state charge distribution. From this pattern, we made an initial assignment (before the availability of the single-tryptophan mutants) of the 415-nm peak to Trp19 and the 407-nm peak to Trp99. However, there are exceptions to this pattern, such as ribonuclease T_1, which has a single, interior tryptophan residue and which shows a very blue 0–0 phosphorescence transition (Hershberger *et al.*, 1980; Lam *et al.*, 1992). Consequently, while phosphorescence 0–0 band position generally is a reliable indicator of the tryptophan microenvironment, exceptional circumstances may result in deviations from this trend. The single-tryptophan mutants clearly show that Trp19 (in W99F) is responsible for the 407-nm peak in WT and that Trp99 (in W19F) is responsible for the 415-nm peak. Thus, on comparison with the X-ray structure, the 415-nm peak is associated with the more solvent exposed residue in trpR. Both the room temperature fluorescence and the low-temperature phosphorescence suggest that Trp19 is at least moderately solvent exposed. This is in agreement with the X-ray structure. The ODMR zfs parameters are also found to be different for Trp19 and Trp99 and to provide some insight into the microenvironment of these residues. These zfs parameters will be discussed in the next subsection.

While the assignment is easily made on the basis of the phosphorescence spectra, parameters obtained from steady-state and time-resolved fluroescence studies are also consistent with the assignment of the redder fluorescing (and absorbing), shorter lived, more mobile and solvent exposed fluorescent component to Trp99 and the bluer fluorescing (and absorbing), longer lived, less mobile and less solvent exposed fluorescent component to Trp19. In the following section we will discuss further the luminescence characteristics of each type of tryptophan residue.

Luminescence Characteristics of Each Residue. The fluorescence of Trp99 of trpR is moderately red (λ_{max} = 338 nm), consistent with it being near the surface of the protein. The absorbance of Trp99 extends to longer wavelengths than does that of Trp19. Since the electronic dipole of indole is much larger in the excited singlet state, the red absorbance of Trp99 is consistent with effective interaction of the excited state of this residue with surrounding solvent molecules and/or polar side chains. The low quantum yield and mean fluroescence lifetime of Trp99 indicate that there are quenching amino acid side chains in its environment. Royer (1992) has suggested that nearby glutamine and asparagine residues are likely to be responsible for the intramolecular quenching. Whatever the quenching mechanism for Trp99, the fluorescence decay of this residue (in W19F) is nonexponential, as has been found for other surface tryptophan residues in proteins and peptides (Ross *et al.*, 1981; Cockle & Szabo, 1981). The rate constants for solute quenching by acrylamide and iodide are large for tryptophan residues in proteins (compare to the list of k_q values in Table III of Eftink (1991b)), indicating the exposure of Trp99. This residue has a significant degree of rotational freedom, as indicated by a large contribution to the anisotropy decay data from a subnanosecond rotational correlation time. The anisotropy decay data, analyzed in terms of the "model free" model of Lipari and Szabo (1980), are

consistent with this residue being able to rotate independently from the protein within a cone of semi-angle 45°.

The fluorescence of Trp19 is relatively blue and has the higher intrinsic quantum yield. In W99F the fluorescence decay of Trp19 is very close to being a monoexponential (>95% of the fluorescence associated with a 3.94-ns component). In WT, the decay time of Trp19 appears to be slightly reduced to 3.36 ns (see next section). This tryptophan residue is not deeply buried, however, as evidenced by the acrylamide and iodide quenching rate constants in the range $1–1.6 \times 10^9$ M^{-1} s^{-1}. The fact that the iodide k_q is larger than the acrylamide k_q is unusual and suggests that nearby positively charged amino acid side chains may facilitate quenching by iodide. Trp19 has essentially no freedom of rotation, with respect to the protein; the rotational correlation time for Trp19 in W99F is approximately the value that is expected for global rotation of a protein the size of the trpR dimer.[2]

The results regarding the triplet state of the two tryptophan residues shows their environments to be significantly different. Moreover, while the above fluorescence information leads to the view that both types of residues are exposed to solute quenchers, with Trp99 having the greater degree of exposure, the low-temperature phoshorescence and ODMR data indicate that this view is something of an oversimplification. The 0–0 transitions of both Trp19 and Trp99 are very sharp (see Figure 4), suggesting that they each have a relatively homogeneous environment. The $2E$ and $D - E$ zfs parameters show a significant wavelength dependence, however, which indicates that the environment of each residue has some heterogeneity. The greater wavelength dependence of the ODMR frequency, as well as the larger ODMR line width of Trp19, suggests that this residue has a more heterogeneous microenvironment.

At the low temperature required for phosphorescence and ODMR studies, relaxation of solvent molecules and polar side chains, in response to the large electronic dipole of the excited triplet state, will be frozen. The 0–0 wavelength and the zfs parameters for Trp19 of W99F exhibit a typical pattern for an exterior tryptophan residue. Thus, the phosphorescence and ODMR parameters indicate that the environment of the triplet state of Trp19 is relatively destabilizing (compared to that of Trp99) and appears to be rigid and nonrelaxing at low temperature. (Note that the fluorescence data do not characterize Trp19 as being buried to either ionic or neutral quenchers.) The observation that, in WT, the 407-nm peak of Trp19 is only about one-third the amplitude of the 415-nm peak of Trp99 will be discussed in the next section.

The wavelength of the 0–0 phosphorescence transition of a tryptophan residue in a polarizable, hydrophobic interior of a protein is usually found to the red of a solvent-exposed residue. Also, the $D - E$ and $2E$ ODMR frequencies are usually found to be smaller and larger, respectively, for a buried residue, compared to the zfs parameters for a solvent-exposed residue. There are, however, anomalous cases, such as the internal trytophan in ribonuclease T_1, which deviate from this pattern (Hershberger *et al.*, 1980). The phosphorescence and ODMR data for Trp99 resemble those of a typical interior residue, whereas the fluorescence data show it to be relatively exposed to quenchers and solvent. These opposing results might indicate that the environment of Trp99 stabilizes the excited triplet state, possibly due to the polarizability of groups around this indole ring, or perhaps protein conformational changes

Scheme I

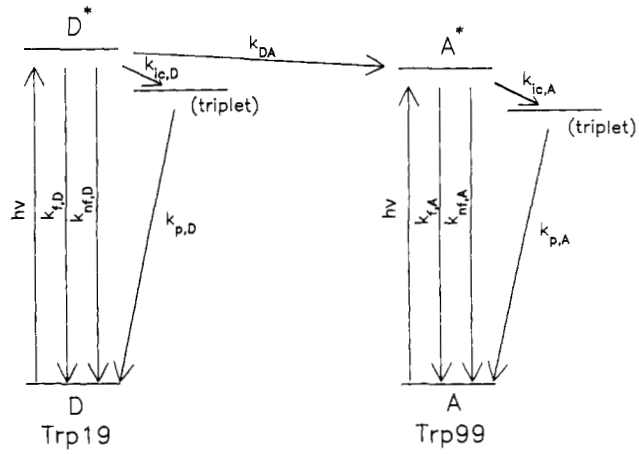

occur upon freezing that occlude solvent molecules from the Trp99 local environment. On the other hand, local, polar groups may be arranged such that the excited triplet state dipole of Trp99 is fortuitously stabilized relative to the ground state, leading to a very red-shifted 0–0 band. An unusual environment of Trp99 is suggested by the larger wavelength dependence of the zfs parameters (Figure 6) than is typically found for a residue buried in a polarizable microenvironment, e.g., Trp138 of T4 lysozyme (Ghosh *et al.*, 1988).

Evidence for Energy Transfer between Tryptophan Residues. The possibility of homotransfer between tryptophan residues in a protein must be considered. It is difficult to experimentally support the existence of homotransfer, but the availability of a two-tryptophan protein (WT) and of single-tryptophan mutants makes possible some characterization of this energy-transfer process. Several results with trpR suggest to us that homotransfer occurs in WT. These results are (i) time-resolved fluorescence data for the longer τ in WT and W99F, (ii) fluorescence quantum yield data for WT that are lower than expected, and (iii) the observation that the 407-nm phosphorescence peak is anomalously weak relative to the 415-nm peak. These results will be discussed below.

For a macromolecule having two luminescing centers, such as Trp19 and Trp99 (see Scheme I), for which irreversible energy transfer can occur from the donor (D) center to the acceptor (A) center, the fluorescence decay time will be (at least) a biexponential process. The apparent fluorescence decay time of the donor will be decreased by the k_{DA} term ($1/\tau_D = k_{f,D} + \sum k_{nf,D} + k_{ic,D} + k_{DA}$) compared to the decay rate in the absence of the energy-transfer process ($1/\tau_D = k_{f,D} + \sum k_{nr,D} + k_{ic,D}$). (See Scheme I for definitions of the rate constants.) The preexponential associated with τ_D will be reduced by the energy-transfer process. (In favorable cases, one can even see a negative preexponential associated with τ_D in some wavelength regions (Badea & Brand, 1979; Eftink, 1991a). Of course, the decay of D and A may be intrinsically nonexponential.) The decay time of the acceptor will be $1/\tau_A = k_{f,A} + \sum k_{nf,A} + k_{ic,A}$, as it is in the absence of the energy-transfer term, and the preexponential associated with τ_A will be larger. Comparing the τ_i and α_i values for WT and the two mutants in Table I, we find that the long τ_1 drops from 3.94 ns in W99F to 3.36 ns in WT. This drop in τ_1 is consistent with the occurrence of energy transfer between Trp19 as donor and Trp99 as acceptor. However, we have considered only a biexponential decay fit for the data in Figure 3. An analysis for more components could be attempted, as was done by Royer (1992). The fact that Trp99 has a minor 3-ns component complicates matters, however. It is worth noting

[2] We observed no evidence for the aggregation of trpR dimers, as demonstrated in the work of Fernando and Royer (1992). However, we have worked at an ionic strength of ~0.2; the aggregation effects appear to be more significant at low ionic strength.

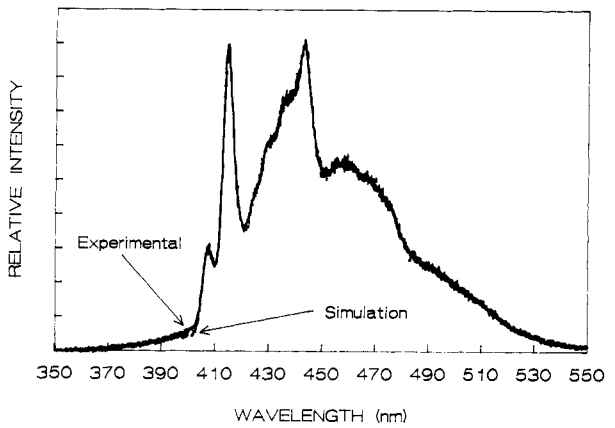

FIGURE 8: Simulation of the phosphorescence spectrum of WT trpR by a linear superposition of the normalized spectra for W19F and W99F. The experimental WT trpR spectrum and the simulated spectrum are shown superimposed. The simulated spectrum was obtained using 0.75 part of the W19F spectrum and 0.25 part of the W99F spectrum. The simulation is so good that it can hardly be distinguished from the experimental spectrum of WT.

that Royer also suggested that Trp19 to Trp99 energy transfer occurs from a consideration of the preexponential values associated with the decay time assigned to Trp19 in WT.

The fluorescence quantum yield of WT is less than expected from the sum of the quantum yield data for the two mutants. In the absence of energy transfer between the tryptophan residues, the quantum yield, Φ, of the protein is expected to be $\Phi = \alpha_{19}\Phi_{19} + \alpha_{99}\Phi_{99}$, where Φ_{19} and Φ_{99} are taken as the quantum yields of these remaining tryptophan residues in the mutants W99F and W19F, respectively, and α_{19} and α_{99} are the normalized relative absorbances of the two residues at the excitation wavelength (α is used for the latter parameter since it is analogous to the preexponential α in eq 2). From the absorption spectra in Figure 1B we calculate α_{19} and α_{99} to be 42% and 58% at an excitation wavelength of 295 nm. With these values, we calculate an expected $\Phi = 0.091$ for WT in the absence of energy transfer. The measured value of 0.063 is significantly lower than this calculated value. If energy transfer occurs, then the quantum yield of WT will be given by the following equation, where E_T is the efficiency of energy transfer from Trp19 to Trp99.

$$\Phi = \alpha_{19}\Phi_{19}(1 - E_T) + \alpha_{99}\Phi_{99}(1 + E_T\alpha_{19}/\alpha_{99}) \quad (4)$$

Again, making the assumption that the values of Φ for the mutants can be taken as Φ_{19} and Φ_{99} and from the experimental Φ for WT, we calculate the energy-transfer efficiency to be 54%. This analysis depends on the assumed values of Φ_{19} and Φ_{99}, from the two single-tryptophan mutants (i.e., it assumes that the environments of the tryptophan residues are the same in the mutant and WT proteins), but the calculated E_T supports the notion that there is a significant degree of energy transfer in the protein.

The observation that the 415-nm phosphorescence peak is approximately 3 times the height of the 407-nm peak is also supportive of energy transfer from Trp19 (the 407-nm peak) to Trp99 (the 415-nm peak). In addition to comparing the heights of the resolved 0–0 peaks, we have also quantitated the two component spectra by simulating the WT phosphorescence as a combination of the spectra of W19F and W99F. Figure 8 shows that the WT spectrum can be simulated with a ratio of 3 parts of Trp99 (in W19F) and 1 part of Trp19 (in W99F). At 77 K almost all of the thermal quenching processes (k_{nf} and k_{np} in Scheme I) for the excited singlet and triplet states have diminished. The phosphorescence quantum yield on an individual emitting center (i.e., Trp19 in W99F) is $\Phi_p = k_{ic}\tau_f k_p/(k_p + k_{np})$ in the absence of energy transfer, where the rate constants are defined in Scheme I and where the fluorescence lifetime, τ_f, equals $(k_f + \sum k_{nf} + k_{ic})^{-1}$, or $(k_f + \sum k_{nf} + k_{ic} + k_{DA})^{-1}$ if energy transfer occurs. Thus, the existence of energy transfer from Trp19 to Trp99 would result in a lower phosphorescence quantum yield for Trp19 than for Trp99, with the phosphorescence decay time, $\tau_p = (k_p + k_{np})^{-1}$, being the same for both the donor and the acceptor. From the ratio (3.0) of the component spectra we estimate the efficiency of energy transfer, E_T, to be approximately 50%. (See Addendum.) Note that this energy transfer is at the singlet level, even though it is estimated from phosphorescence data, and that the E_T value is in surprisingly good agreement with the value determined from room temperature fluorescence quantum yield data. Quantitative agreement should not be expected, since E_T may differ for fluid and rigid solvent media (Ghosh *et al.*, 1988).

ACKNOWLEDGMENT

We thank Dr. Kathleen Matthews, Rice University, for supplying the wild-type protein and Dr. Dana Hu, University of Mississippi, for helping with the protein isolation. We also thank Dr. Cathy Royer, University of Wisconsin, for sharing her results with us and for helpful conversations.

ADDENDUM: ENERGY-TRANSFER AND STEADY-STATE PHOSPHORESCENCE DATA

Consider the system described by Scheme I in which there is unidirectional energy transfer between excited singlet states of two similar chromophores on a macromolecule (i.e., Trp19 and Trp99 of trpR). Under low-level steady-state illumination and at relatively dilute concentrations of the macromolecule (so that intermolecular interactions can be neglected), the phosphorescence quantum yield of the donor, D, and acceptor, A, is given by

$$\Phi_{p,D} = \alpha_D[k_{ic,D}/(k_{f,D} + \sum k_{nf,D} + k_{ic,D} + k_{DA})][k_{p,D}/(k_{p,D} + \sum k_{np,D})] \quad (1A)$$

$$= \alpha_D[k_{ic,D}/(k_{f,D} + \sum k_{nf,D} + k_{ic,D})](1 - E_T)[k_{p,D}/(k_{p,D} + \sum k_{np,D})] \quad (2A)$$

$$= \alpha_D\Phi_{ic,D}(1 - E_T)\Phi_{p,D}' \quad (3A)$$

and

$$\Phi_{p,A} = \alpha_A[k_{ic,A}/(k_{f,A} + \sum k_{nf,A} + k_{ic,A})][k_{p,A}/(k_{p,A} + \sum k_{np,A})] + \alpha_D[k_{DA}/(k_{f,D} + \sum k_{nf,D} + k_{ic,D} + k_{DA})][k_{ic,A}/(k_{f,A} + \sum k_{nf,A} + k_{ic,A})][k_{p,A}/(k_{p,A} + \sum k_{np,A})] \quad (4A)$$

$$= \alpha_A\Phi_{ic,A}\Phi_{p,A}' + \alpha_D E_T\Phi_{ic,A}\Phi_{p,A}' \quad (5A)$$

$$= \alpha_A\Phi_{ic,A}(1 + E_T\alpha_D/\alpha_A)\Phi_{p,A}' \quad (6A)$$

where $E_T = k_{DA}/(k_{f,D} + \sum k_{nf,D} + k_{ic,D} + k_{DA})$, $\Phi_{ic,D} = k_{ic,D}/(k_{f,D} + \sum k_{nf,D} + k_{ic,D})$ (i.e., $\Phi_{ic,D}$ is defined for the absence of energy transfer, and the effective $\Phi_{ic,D}$ when energy transfer exists is $\Phi_{ic,D}(1 - E_T)$), $\Phi_{ic,A} = k_{ic,A}/(k_{f,A} + \sum k_{nf,A} + k_{ic,A})$, $\Phi_{p,D}' = k_{p,D}/(k_{p,D} + \sum k_{np,D})$, and $\Phi_{p,A}' = k_{p,A}/(k_{p,A} + \sum k_{np,A})$. The α_D and α_A values are the fractional relative absorbance values (analogous to the preexponentials in eq 2) for the D and A chromophores.

If there is no intrinsic quenching of the triplet state (i.e., $\sum k_{np} = 0$, which is the case at low temperature where the phosphorescence decay time of tryptophan residues is at its maximum value of 5–6 s), then $\Phi_{p,D}' = \Phi_{p,A}' = 1.0$ and the above equations simplify as follows.

$$\Phi_{p,D} = \alpha_D \Phi_{ic,D}(1 - E_T) \quad (7A)$$

$$\Phi_{p,A} = \alpha_A \Phi_{ic,A}(1 + E_T \alpha_D/\alpha_A) \quad (8A)$$

If the phosphorescence contributions of the donor and acceptor can be resolved (as in the case of Trp19 and Trp99 in trpR), then the ratio of the contributions from the acceptor and donor are

$$\Phi_{p,A}/\Phi_{p,D} = \alpha_A \Phi_{ic,A}(1 + E_T \alpha_D/\alpha_A)/\alpha_D \Phi_{ic,D}(1 - E_T) \quad (9A)$$

If (i) the measurements are made at low temperature such that $k_{nf} = 0$, and if (ii) the intrinsic fluorescence and intersystem crossing rate constants, k_f and k_{ic}, are approximately the same for both donor and acceptor, then the above equation becomes

$$\Phi_{p,A}/\Phi_{p,D} = (\alpha_A/\alpha_D)(1 + E_T \alpha_D/\alpha_A)/(1 - E_T) \quad (10A)$$

Further, if the fractional absorbances of the acceptor and donor are approximately the same at the excitation wavelength, eq 10A can be approximated as

$$\Phi_{p,A}/\Phi_{p,D} \approx (1 + E_T)/(1 - E_T) \qquad (\text{when } \alpha_A = \alpha_D) \quad (11A)$$

Equation 10A and its approximation, eq 11A, apply when the 0–0 transitions for two tryptophan residues can be resolved so that the ratio $\Phi_{p,A}/\Phi_{p,D}$ can be easily determined. If, however, the 0–0 transitions are not completely resolved, an analysis is possible if single-tryptophan-containing mutant proteins are available. As one of our groups has shown previously (Ghosh *et al.*, 1988), by measurement of the relative intensity of 0–0 transitions for equimolar concentrations of a two-tryptophan WT and single-tryptophan mutants, a normalized ratio, $(\Phi_{p,A}{}^{WT}/\Phi_{p,A}{}^{mut})/(\Phi_{p,D}{}^{WT}/\Phi_{p,D}{}^{mut})$, can be obtained. In our study with trpR, the values of $\Phi_{p,A}{}^{WT}$ and $\Phi_{p,D}{}^{WT}$ can be obtained by curve fitting using the spectra of the mutants, as we have done in Figure 8, so that complete resolution is not required (see Ghosh *et al.*, 1988). By using such a normalized ratio of data for equimolar concentrations of the proteins, one of the α_A/α_D ratios drops out of eq 10A to give the following:

$$(\Phi_{p,A}{}^{WT}/\Phi_{p,A}{}^{mut})/(\Phi_{p,D}{}^{WT}/\Phi_{p,D}{}^{mut}) = (1 + E_T \alpha_D/\alpha_A)/(1 - E_T) \quad (12A)$$

An analogous, inverted form of this equation was presented as eq 1 in Ghosh *et al.* (1988). The latter equation should have contained the α_D/α_A factor, as above. Again, if $\alpha_A \approx \alpha_D$, then eq 12A simplifies to $(1 + E_T)/(1 - E_T)$.

Applying these equations to experimental data, we see that, for the case of Trp19 and Trp99 in trpR, the normalized ratio of the contributions of these two residues to the phosphorescence spectrum is 3.0 (see Figure 8). Using eq 12A with the approximation that $\alpha_A \approx \alpha_D$, the value of the degree of energy transfer, E_T, is calculated to be 50%. Considering other published studies, phosphorescence data for horse liver alcohol dehydrogenase shows no evidence of energy transfer between its two tryptophan residues, since there is a nearly equal phosphorescence contribution (at low temperature) from its Trp15 and Trp314 residues (Purkey & Galley, 1970). Bacteriophage T4 lysozyme and its mutants show clear evidence of energy transfer (i.e., between Trp126 and Trp158 and, to a lesser extent, between Trp126 and Trp138) from observartion of the height of the 0–0 phosphorescence transitions for the individual tryptophan residues (Ghosh *et al.*, 1988).

The addition of a heavy atom perturbant may (a) increase the magnitude of the intersystem crossing rate constants, $k_{ic,D}$ and $k_{ic,A}$, (b) increase the rate constants $k_{p,D}$ and $k_{p,A}$, and (c) contribute to $\sum k_{nf,D}$ and $\sum k_{nf,A}$, the rate constants for nonradiative decay of the single states. The effect of increasing $k_{p,D}$ and $k_{p,A}$ will be to shorten the phosphorescence decay time but not affect the magnitude of $\Phi_{p,D}$ and $\Phi_{p,A}$. The effect of a heavy atom perturbant on $k_{ic,D}$ and $k_{ic,A}$ will be to increase both $\Phi_{ic,D}$ and $\Phi_{ic,A}$, possibly by differing amounts. The effect of the heavy atom perturbant on $\sum k_{nf}$ will be to decrease $\Phi_{ic,D}$ and $\Phi_{ic,A}$ (in opposition to the above effect), but in the case where there is energy transfer, the increase in $\sum k_{nf,D}$ will result in a decrease in E_T. A consequence of the latter is that the dominant effect of a heavy atom perturbant will probably be to decrease the ratio $\Phi_{p,A}/\Phi_{p,D}$ in eqs 9A and 10A. In the case of trpR, addition of KI was found to enhance the phosphorescence intensity of both the 407- and 415-nm peaks, but to increase the intensity of the former (donor Trp19) peak to a greater extent, as seen in Figure 5.

REFERENCES

Arrowsmith, C. H., Carey, J., Treat-Clemons, L., & Jardetzky, O. (1989) *Biochemistry 28*, 3875–3879.

Badea, M. G., & Brand, L. (1979) *Methods Enzymol. 61*, 378–425.

Beechem, J. M., Gratton, E., Ameloot, M., Knutson, J. R., & Brand, L. (1991) in *Principles of Fluorescence Spectroscopy* (Lakowicz, J. R., Ed.) Vol. 2, pp 241–306, Plenum Press, New York.

Carey, J. (1988) *Proc. Natl. Acad. Sci. U.S.A. 85*, 975–979.

Chou, W.-Y., Bieber, C., & Matthews, K. S. (1989) *J. Biol. Chem. 264*, 18309–18313.

Cockle, S. A., & Szabo, A. G. (1981) *Photochem. Photobiol. 34*, 23–27.

Eftink, M. R. (1991a) *Methods Biochem. Anal. 35*, 127–205.1.

Eftink, M. R. (1991b) in *Topics in Fluorescence Spectroscopy*, (Lakowicz, J. R., Ed.) Vol. 2, pp 53–127, Plenum Press, New York.

Eftink, M. R. (1992) in Advances in Biophysical Chemistry (Bush, C. A., Ed.) Vol. 2, pp 81–114, JAI Press, Greenwich, CT.

Eftink, M. R. & Ghiron, C. A. (1976) *Biochemistry 15*, 672–680.

Fernando, T., & Royer, C. A. (1992) *Biochemistry 31*, 3429–3441.

Ghosh, S., Zang, L.-H., & Maki, A. H. (1988) *J. Chem. Phys. 88*, 2769–2775.

Hershberger, M. V., Maki, A. H., & Galley, W. C. (1980) *Biochemistry 19*, 2204–2209.

Joachimiak, A., Kelley, R. L., Gunsalus, R. P., & Yanofsky, C. (1983) *Proc. Natl. Acad. Sci. U.S.A. 80*, 668–672.

Kwiram, A. L., & Ross, J. B. A. (1982) *Annu. Rev. Biophys. Bioeng. 11*, 223–249.

Lam, W.-C., Maki, A. H., Itoh, T., & Hakoshima, T. (1992) *Biochemistry 31*, 6751–6760.

Lawson, C. L., & Sigler, P. B. (1988) *Nature 333*, 869–871.

Li, Z., Rappaport, A., & Galley, W. C. (1992) *Biophys. J. 61*, a181.

Lipari, G., & Szabo, A. (1980) *Biophys. J. 30*, 489–506.

Maik, A. H. (1984) *Biol. Magn. Reson. 6*, 187–293.

Mann, C. J., Royer, C. A., & Matthews, C. R. (1993) *Protein Sci.* (submitted for publication).

Marmorstein, R. Q., & Sigler, P. B. (1989) *J. Biol. Chem. 264*, 9149–9154.

Marmorstein, R. Q., Joachimiak, A., Spring, M., & Sigler, P. (1987) *J. Biol. Chem. 262*, 4922–4927.

Otwinowski, Z., Schevitz, R.-G., Zhang, C. L., Lawson, C. L., Joachimiak, A., Marmorstein, R. Q., Luisi, B. F., & Sigler, P. B. (1988) *Nature 335*, 321–329.

Paluh, J. L., & Yanofsky, C. (1986) *Nucleic Acids Res. 14*, 7851–7860.

Purkey, R. M., & Galley, W. C. (1970) *Biochemistry 9*, 3569–3575.

Ross, J. B. A., Rousslang, K., & Brand, L. (1981) *Biochemistry 20*, 4361–4369.

Royer, C. A. (1992) *Biophys. J. 63*, 741–750.

Royer, C. A., Gardner, J. A., Beechem, J. M., Brochon, J.-C., & Matthews, K. S. (1990) *Biophys. J. 58*, 363–378.

Von Shutz, J. U., Zuclich, J. A., & Maki, A. H. (1974) *J. Am. Chem. Soc. 96*, 714–718.

Zhang, R.-G, Joachimiak, A., Lawson, C. L., Schevitz, R. W., Otwinowski, Z., & Sigler, P. B. (1987) *Nature 327*, 591–597.

Zurawski, G., Gunsalus, R. P., Brown, K. D., & Yanofsky, C. (1981) *J. Mol. Biol. 145*, 47–73.